

BABAR B DECAY RESULTS

JORDAN NASH

*Blackett Laboratory,**Imperial College,**South Kensington,**LONDON SW7 2BW, United Kingdom**E-mail: j.nash@ic.ac.uk**on behalf of the BABAR collaboration*

Data from the first run of the *BABAR* detector at the PEP II accelerator are presented. Measurements of many rare B decay modes are now possible using the large data sets currently being collected by *BABAR*. An overview of analysis techniques and results on data collected in 2000 are described.

1 Introduction

The *BABAR* detector¹ began collecting data just over two years ago with the heart of our physics program centered around the search for CP violation in the B meson system. The excellent performance of the PEP II accelerator has allowed us to establish the existence of CP violation in B decays as Jonathan Dorfan has shown today^{2,3}, and also seen by our colleagues at KEK⁴. In searching for CP violation, it is necessary to perform a series of measurements of rare B decay modes which establish the ability of the detector to accurately determine the parameters of CP violation. These measurements also provide an opportunity to look for rare decays which could give a hint of physics beyond the Standard Model. In addition, many of the modes which are now rare modes will provide independent measurements of CP violating effects during the high luminosity era of the B factories.

This talk will provide a taste of the physics program which is just now starting at *BABAR*. The results presented here are based on the first Run of *BABAR* which lasted until December 2000 and collected $20.7/fb$ of data on the peak of the $\Upsilon(4S)$ resonance (approximately 22.7 million $B\bar{B}$ pairs), and $2.6/fb$ data off-peak. Most results are preliminary.

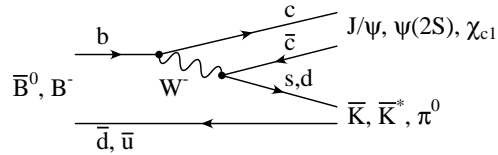


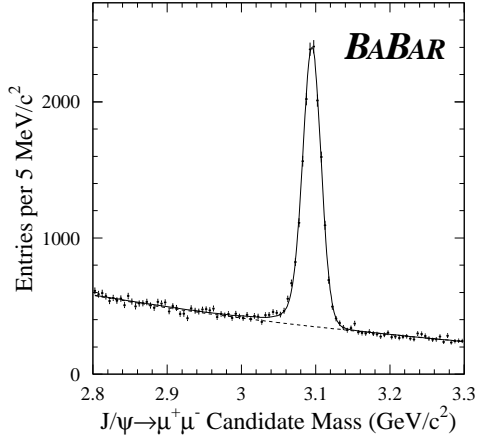
Figure 1. Feynman diagram for B meson decays to charmonium.

2 B Decays with Charmonium

The majority of the modes which went into the measurement of $\sin 2\beta$ include charmonium in the final state. An important first step was to improve measurements of B mesons into final states including charmonium, as well as establishing measurements of the B into previously unseen modes.

2.1 Inclusive Cross Sections

Charmonium is produced in B decays primarily through the internal spectator diagram shown in figure 1. The J/ψ is detected in the leptonic decay channels to electrons and muons. An example of the inclusive measurement of charmonium production is shown in figure 2. The inclusive branching fractions for B decays to final states including charmonium are determined to be $\mathcal{B}(B \rightarrow J/\Psi X) = (1.044 \pm 0.013 \pm 0.028) \times 10^{-2}$, $\mathcal{B}(B \rightarrow \psi(2S)X) = (0.275 \pm 0.020 \pm 0.029) \times 10^{-2}$, $\mathcal{B}(B \rightarrow \chi_{c1}X) = (0.378 \pm 0.034 \pm 0.026) \times$

Figure 2. Inclusive J/ψ decays into muons.

10^{-2} . In addition, we have also observed the production of charmonium in the continuum at a rate $\sigma_{e^+e^- \rightarrow J/\psi X} = 2.52 \pm 0.21 \pm 0.21 \text{ pb}^5$ which is the first such measurement.

2.2 Exclusive Cross Sections

In order to determine the exclusive cross sections for B decays we use two main kinematic variables which take advantage of the fact that the B mesons are produced nearly at rest in the $\Upsilon(4S)$ rest frame, and that the beam energy is well determined.

The energy-substituted mass $m_{ES} \equiv \sqrt{E_{Beam}^{*2} - p_B^{*2}}$ uses the beam energy and the reconstructed B momentum to form an effective mass for the B candidate. The mass resolution for m_{ES} is approximately 2 – 3 MeV and the particle mass hypothesis is not needed. B events should peak at the B mass in this variable. $\Delta E \equiv E_B^* - E_{Beam}^*$ is an orthogonal variable which takes into account the particle mass hypothesis. It has a resolution of approximately 10 – 20 MeV depending on the decay mode, and should be centered at 0 if the particle hypotheses are correct. These two kinematic variables are used in nearly all of our exclusive B decay analyses.

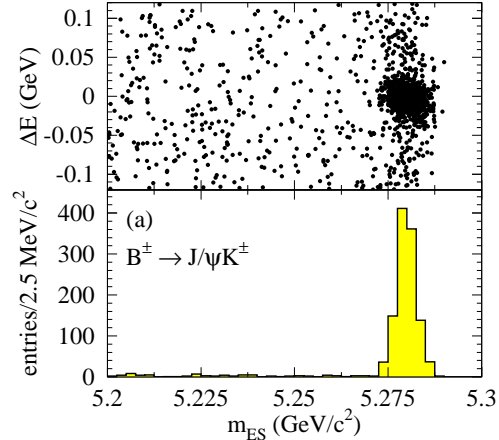
Figure 3. ΔE vs m_{ES} for the decay $B^+ \rightarrow J/\psi K^+$ the bottom figure shows the projection of m_{ES} where a cut has been made on ΔE .

Figure 3 shows ΔE plotted against m_{ES} for the decay mode $B^+ \rightarrow J/\psi K^+$. A selection is made for ΔE centered around 0, and the projection is shown in the bottom of the figure for the variable m_{ES} . There is a clear signal with very low background. The sidebands in m_{ES} are used to estimate the backgrounds under the B peak which are small in most of the decay modes. Figure 4 shows an example of the projection of ΔE for one mode.

Exclusive branching fractions for many B decay modes with charmonium in the final state have been measured⁶ and are summarized in table 1. In most of these modes, the backgrounds are small and are estimated using the sidebands. Backgrounds are primarily from other B decays which contain charmonium, and these cross-feeds are estimated using the simulation.

In addition to these branching fraction measurements, we also present a measurement of the ratio $\mathcal{B}(B^\pm \rightarrow J/\psi \pi^\pm)/\mathcal{B}(B^\pm \rightarrow J/\psi K^\pm) = [3.91 \pm 0.78 \pm 0.19]\%$ ⁷, which significantly improves upon previous measurements, and is in good agreement with theoretical predictions.

Table 1. Branching fraction results for B decays to final states containing charmonium.

Channel		Branching fraction/ 10^{-4}		
$B^0 \rightarrow J/\psi K^0$	$K_S^0 \rightarrow \pi^+ \pi^-$	8.5	± 0.5	± 0.6
	$K_S^0 \rightarrow \pi^0 \pi^0$	9.6	± 1.5	± 0.7
	K_L^0	6.8	± 0.8	± 0.8
	All	8.3	± 0.4	± 0.5
$B^+ \rightarrow J/\psi K^+$		10.1	± 0.3	± 0.5
$B^0 \rightarrow J/\psi \pi^0$		0.20	± 0.06	± 0.02
$B^0 \rightarrow J/\psi K^{*0}$		12.4	± 0.5	± 0.9
$B^+ \rightarrow J/\psi K^{*+}$		13.7	± 0.9	± 1.1
$B^0 \rightarrow \psi(2S)K^0$		6.9	± 1.1	± 1.1
$B^+ \rightarrow \psi(2S)K^+$		6.4	± 0.5	± 0.8
$B^0 \rightarrow \chi_{c1}K^0$		5.4	± 1.4	± 1.1
$B^+ \rightarrow \chi_{c1}K^+$		7.5	± 0.8	± 0.8
$B^0 \rightarrow \chi_{c1}K^{*0}$		4.8	± 1.4	± 0.9

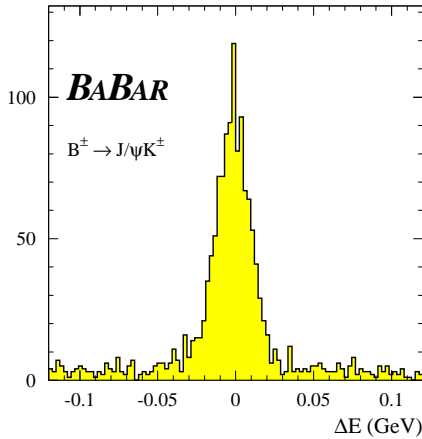


Figure 4. ΔE projection for the decay $B^\pm \rightarrow J/\psi K^\pm$.

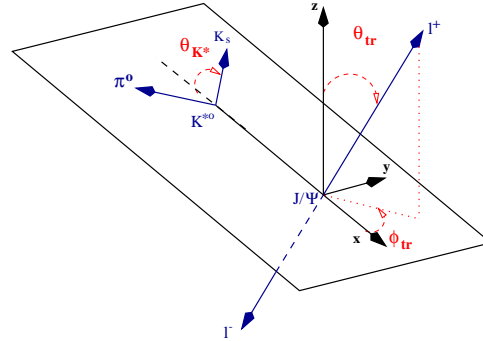


Figure 5. Definition of the angles used to extract the relative amplitudes in the decay $B^0 \rightarrow J/\psi K^*$.

2.3 Angular Analysis of $B^0 \rightarrow J/\psi K^*$

One exclusive mode deserves a little more discussion. The decay mode $B^0 \rightarrow J/\psi K^*$ is used to measure $\sin 2\beta$; however as this mode contains a mixture of odd and even CP amplitudes, it is necessary to determine the relative contribution of odd and even CP final states. This can be accomplished by the use of an angular analysis of the decay.

BABAR has used a transversity analysis, looking at the decay angles of the K^* and the J/ψ ⁸. Figure 5 shows the angles used to unfold the relative amplitudes. The angular distributions are shown in figure 6, and the

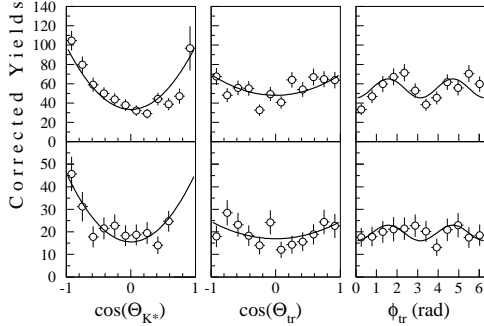


Figure 6. Fit to angular distributions in the decay $B^0 \rightarrow J/\psi K^*$ which allow the extraction of the odd and even CP amplitudes in the decay.

Table 2. Results for the odd and even CP amplitudes in the decay $B^0 \rightarrow J/\psi K^*$.

Quantity	Value
$ A_0 ^2$	$0.597 \pm 0.028 \pm 0.024$
$ A_\perp ^2$	$0.160 \pm 0.032 \pm 0.014$
$ A_\parallel ^2$	$0.243 \pm 0.034 \pm 0.017$
ϕ_\perp (rad)	$-0.17 \pm 0.16 \pm 0.07$
ϕ_\parallel (rad)	$2.50 \pm 0.20 \pm 0.08$

results for CP = +1 states ($|A_0|^2$ and $|A_\parallel|^2$) and CP = -1 state ($|A_\perp|^2$) are tabulated in table 2.

The presence of a significant amplitude of the CP = -1 state dilutes the measured CP in this state by an amount $D = 1 - 2|A_\perp|^2$. The value measured for $|A_\perp|^2$ implies the dilution factor $D = 0.68 \pm 0.10$. This factor is used when the $B^0 \rightarrow J/\psi K^*$ are included in the $\sin 2\beta$ analysis.

3 B Decays with Open Charm

Decays involving open charm ($D^{(*)}$) allow measurement of either the Cabibbo-allowed $b \rightarrow ccs$ decay or the Cabibbo-suppressed $b \rightarrow ccd$ decay. The latter provides another opportunity to measure $\sin 2\beta$ which is complementary to the measurement made with the charmonium modes.

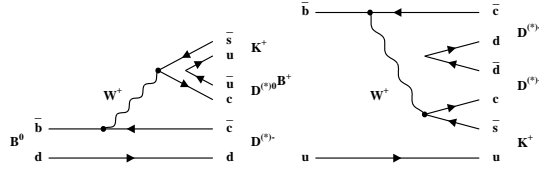


Figure 7. External (left) and internal (right) spectator diagrams for the decays $B \rightarrow D^{(*)} \bar{D}^{(*)} K$.

3.1 $B \rightarrow D^{(*)} \bar{D}^{(*)} K$ Decays

In $b \rightarrow ccs$ decays, one expects the $D_s^{(*)+}$ to be the dominant decay mode. Previous measurements have however indicated that the $B \rightarrow D^{(*)} \bar{D}^{(*)} K$ decays may have a larger than predicted contribution to the $b \rightarrow ccs$ rate. We have looked for the decays $B \rightarrow D^{(*)} \bar{D}^{(*)} K$ in both inclusive and exclusive modes¹². The decays can occur via both the external diagram shown on the left in figure 7 and the colour-suppressed internal diagram shown on the right.

Figure 8 shows m_{ES} for all B^0 modes. The different decay modes are summed as there can be several candidates in each event due to the large number of decay products. We find for the inclusive branching fractions $\mathcal{B}(B^0 \rightarrow D^{*-} D^0 K^+) = (2.8 \pm 0.7 \pm 0.5) 10^{-3}$, $\mathcal{B}(B^0 \rightarrow D^{*-} D^{*0} K^+) = (6.8 \pm 1.7 \pm 1.7) 10^{-3}$.

In addition, we have also measured the exclusive mode $B^+ \rightarrow D^{*-} D^{*+} K^+$ for which the m_{ES} plot is shown in figure 9. The branching fraction is measured to be $\mathcal{B}(B^+ \rightarrow D^{*-} D^{*+} K^+) = (3.4 \pm 1.6 \pm 0.9) 10^{-3}$. This is the first observation of a colour-suppressed mode not involving charmonium.

3.2 $B^0 \rightarrow D^{*+} D^{*-}$

Decays to two D mesons proceed via Cabibbo-suppressed diagrams as shown in figure 10. This decay mode is sensitive to $\sin 2\beta$. However, as in the decay $B^0 \rightarrow J/\psi K^*$, this is a vector-vector decay mode, and there are both CP-odd and CP-even

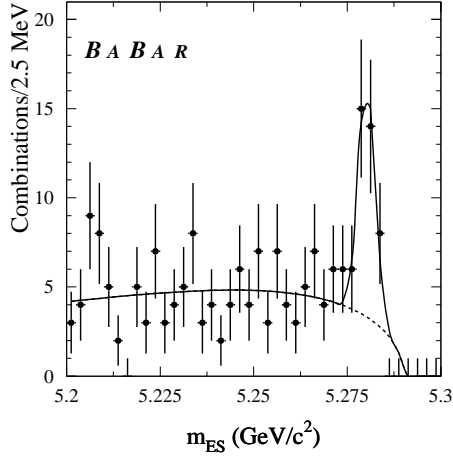


Figure 8. m_{ES} distribution for the decays $B^0 \rightarrow D^{(*)} \bar{D}^{(*)} K$.

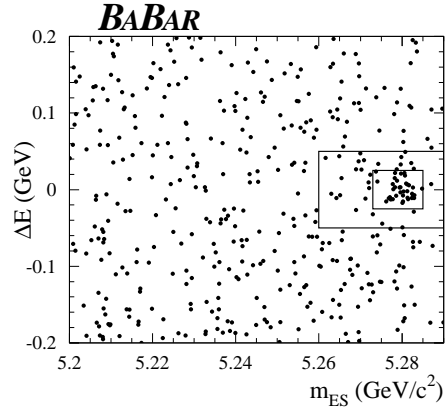


Figure 11. m_{ES} versus ΔE for the decay $B^0 \rightarrow D^{*+} D^{*-}$.

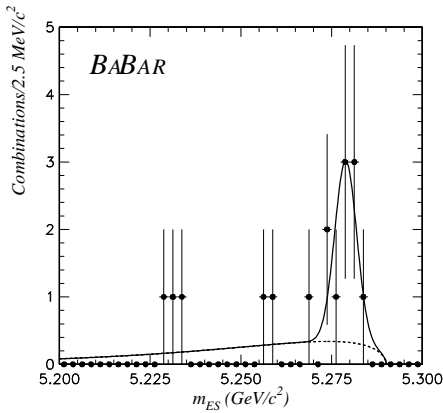


Figure 9. m_{ES} distribution for the exclusive colour-suppressed mode $B^0 \rightarrow D^{*-} D^0 K^+$.

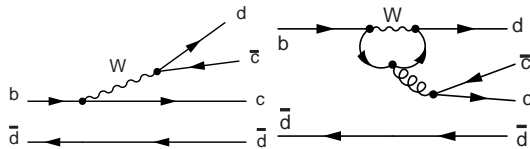


Figure 10. Tree-level diagram (left) and penguin (right) diagrams contributing to $B^0 \rightarrow D^{*+} D^{*-}$ decays.

components. These will need to be measured before $\sin 2\beta$ can be extracted from the data. Again these modes are difficult to reconstruct due to the large number of particles in the final states. The D^* modes offer the most constraints from the mass difference with the soft pion, and so are reconstructed with a reduced background. We have measured the branching fraction for $B^0 \rightarrow D^{*+} D^{*-}$ ¹³ with the next step being the measurement of the amplitudes of the CP components.

The branching fraction for this mode is Cabibbo-suppressed and should be given approximately by

$$\approx \left(\frac{f_{D^{(*)}}}{f_{D_S^{(*)}}} \right) \tan^2 \theta_C \mathcal{B}(B \rightarrow D_S^{(*)} \bar{D}^{(*)})$$

which is of order 0.1%. We reconstruct both $D^{*+} \rightarrow D^0 \pi^+$, $D^{*+} \rightarrow D^+ \pi^0$, with the D^0 in the decay modes $K^- \pi^+$, $K^- \pi^+ \pi^0$, $K^- \pi^+ \pi^+ \pi^-$, $K_S^0 \pi^+ \pi^-$ and the D^+ in the modes $K^- \pi^+ \pi^+$, $K_S^0 \pi^+$, $K^- K^+ \pi^+$.

Background is determined by looking in the sidebands in the m_{ES} vs ΔE plot (figure 11) in the regions outside the signal box, and scaling this by the relative areas of the signal and background regions to estimate the amount of background in the signal box.

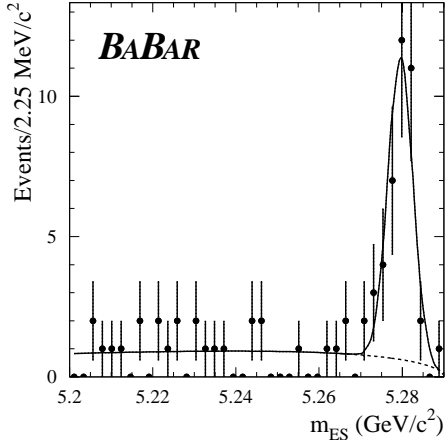


Figure 12. ΔE projection for the decay $B^0 \rightarrow D^{*+}D^{*-}$.

A projection of m_{ES} in the signal box is shown in figure 12. We find a background subtracted signal of $31.8 \pm 6.2 \pm 0.4$ events which gives a branching fraction $\mathcal{B}(B^0 \rightarrow D^{*+}D^{*-}) = (8.0 \pm 1.6 \pm 1.2) \times 10^{-4}$.

The main systematic uncertainties in this analysis come from tracking efficiency (9.4%), due to the large number of tracks in the final state, and the fact that the polarization of the final state is unmeasured (6.6%).

4 Charmless B Decays

One of the most exciting prospects for the coming run will be the start of the process of measuring $\sin 2\alpha$. Charmless B decays are where the B factories will perhaps have their greatest unique advantage in measurements of CKM parameters. *BABAR* have presented the first attempts at these measurements at this conference², which illustrate the prospects and the difficulties in carrying out these measurements.

One of the main difficulties in these measurements is the fact that the penguin diagram (figure 13) contribution is most likely of comparable magnitude to the tree diagram. The implication of this is that one

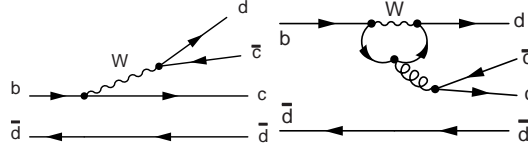


Figure 13. Tree-level diagram (left) and penguin (right) diagrams contributing to charmless B decays.

must determine the relative magnitudes of the two contributions in order to accurately determine the angle $\sin 2\alpha$. One measures an asymmetry which is only an effective $\sin 2\alpha$ and then needs to correct this based on the penguin/tree magnitudes.

There are several strategies for extracting these magnitudes. In the two-body modes, it is possible to perform an isospin analysis which allows one to determine the relative contribution of the penguin and tree diagrams, but it requires the difficult measurements of both $B^0 \rightarrow \pi^0\pi^0$ and $\bar{B}^0 \rightarrow \pi^0\pi^0$. Another strategy involves a full Dalitz plot analysis of the three-body decay modes.

Other difficulties in measuring these modes are the small value of V_{ub} which implies small branching fractions as well as the fact that these modes suffer from severe combinatoric backgrounds.

In addition to measurement of $\sin 2\alpha$, charmless modes also have potential for measurements of direct CP violation as will be discussed in section 7.3.

4.1 Two-body Charmless Decays

Our two-body decay analysis¹⁵ makes use of a maximum likelihood fit where the input to the fit includes a Fisher discriminant based on event shape variables, the m_{ES} and ΔE distributions (shown in figure 14), and the Cherenkov angle measured in the *BABAR* DIRC¹. The DIRC is effective at separating pions from kaons at the high momenta seen in two-body decay modes, and this combined with the measured ΔE provides the ability to distinguish between $B^0 \rightarrow \pi^+\pi^-$

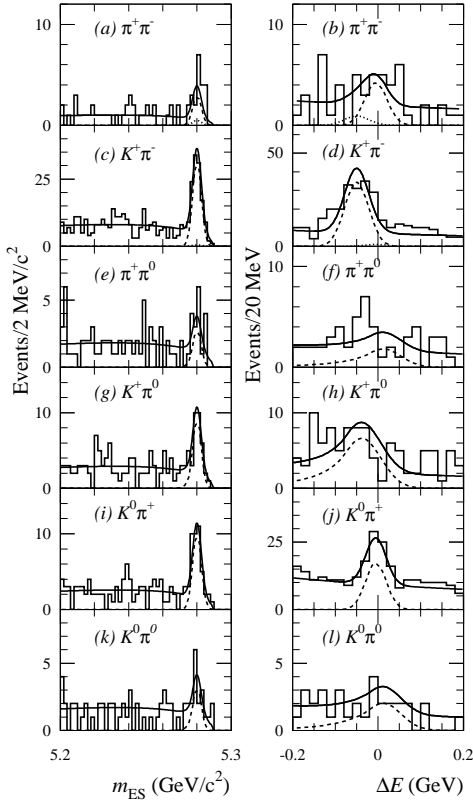


Figure 14. m_{ES} and ΔE projections for charmless two-body B decay modes.

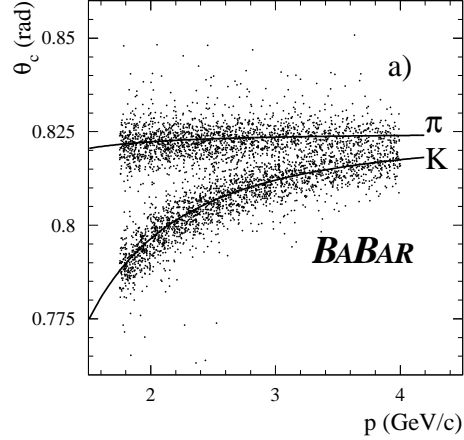


Figure 15. Cherenkov angle measured for pions and kaons as a function of momentum.

Table 3. m_{ES} and ΔE measurements for two-body charmless B decays.

Mode	ϵ (%)	N_S	S (σ)	$B(10^{-6})$
$\pi^+\pi^-$	45	$41 \pm 10 \pm 7$	4.7	$4.1 \pm 1.0 \pm 0.7$
$K^+\pi^-$	45	$169 \pm 17 \pm 13$	15.8	$16.7 \pm 1.6 \pm 1.3$
K^+K^-	43	$8.2^{+7.8}_{-6.4} \pm 3.5$	1.3	< 2.5 (90% C.L.)
$\pi^+\pi^0$	32	$37 \pm 14 \pm 6$	3.4	< 9.6 (90% C.L.)
$K^+\pi^0$	31	$75 \pm 14 \pm 7$	8.0	$10.8^{+2.1}_{-1.9} \pm 1.0$
$K^0\pi^+$	14	$59^{+11}_{-10} \pm 6$	9.8	$18.2^{+3.3}_{-3.0} \pm 2.0$
\bar{K}^0K^+	14	$-4.1^{+4.5}_{-3.8} \pm 2.3$	—	< 2.4 (90% C.L.)
$K^0\pi^0$	10	$17.9^{+6.8}_{-5.8} \pm 1.9$	4.5	$8.2^{+3.1}_{-2.7} \pm 1.2$
$K^0\bar{K}^0$	36	$3.4^{+3.4}_{-2.4} \pm 3.5$	1.5	< 10.6 (90% C.L.)

and $B^0 \rightarrow K^+\pi^-$. Results for the branching fractions measured, and limits on unobserved modes, are summarized in table 3.

4.2 Quasi-two-body Charmless Decays

The CLEO result for the decay branching fraction of $B^+ \rightarrow \eta'K^+$ ¹⁶ was considerably higher than expected from heavy flavour theory¹⁹. We have looked for this decay mode in the Run 1 data. The analysis proceeds¹⁷ by reconstructing η' in the modes $\eta' \rightarrow \eta\pi^+\pi^-$ or $\rho^0\gamma$ and ω in $\omega \rightarrow \pi^+\pi^-\pi^0$. The analysis performs an unbinned maximum likelihood fit on the distributions of $\Delta E, M, m_R, m_\eta$, and a Fisher discriminant based on event shape variables. A significant signal is found in the modes a) $B^+ \rightarrow \eta'K^+$, b) $B^0 \rightarrow \eta'K^0$, and c) $B^+ \rightarrow \omega\pi^+$ which are

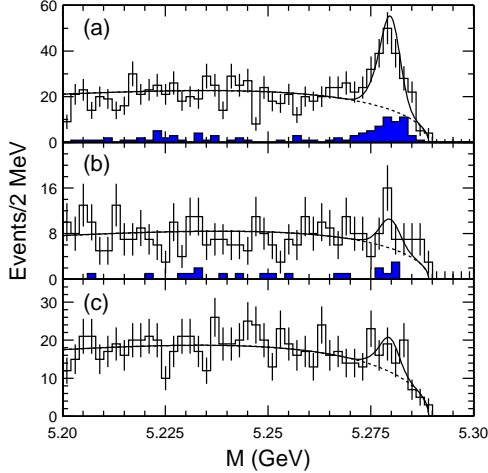


Figure 16. m_{ES} distributions for quasi-two-body decays. The shaded area is $\eta' \rightarrow \eta\pi\pi$.

Table 4. Measured branching fractions and upper limits for quasi two-body B decay modes.

Mode	S	$\mathcal{B}(\times 10^{-6})$ (90% CL)
$\eta'K^+$	17	$70 \pm 8 \pm 5$
$\eta'K^0$	5.9	$42^{+13}_{-11} \pm 4$
$\eta'\pi^+$	2.8	$5.4^{+3.5}_{-2.6} \pm 0.8$ (< 12)
ωK^+	1.6	$1.4^{+1.3}_{-1.0} \pm 0.1$ (< 4)
ωK^0	3.2	$6.4^{+3.6}_{-2.8} \pm 0.8$ (< 12)
$\omega\pi^+$	5.1	$6.6^{+2.1}_{-1.8} \pm 0.7$
$\omega\pi^0$	—	$-4.6 \pm 2.7 \pm 1.2$ (< 4)

shown in figure 16, and the results are summarized in table 4.

4.3 Branching Fractions

$\mathcal{B}(B^0 \rightarrow \eta K^{*0})$ and $\mathcal{B}(B^+ \rightarrow \eta K^{*+})$

Another set of modes with anomalously high branching fractions¹⁸ are $B^0 \rightarrow \eta K^{*0}$ and $B^+ \rightarrow \eta K^{*+}$. These are searched for in the decay modes $\eta \rightarrow \gamma\gamma$, $K^{*0} \rightarrow K^+\pi^-$, and $K^{*+} \rightarrow K_S^0\pi^+$. The analysis²⁰ uses an unbinned maximum likelihood fit using ΔE , $M_{\gamma\gamma}$, $M_{K\pi}$, and a Fisher discriminant based on event shape variables. The B candidate mass is calculated using a full kinematic fit for the mass of the B including the beam energy constraint, m_{EC} . The results for m_{EC}

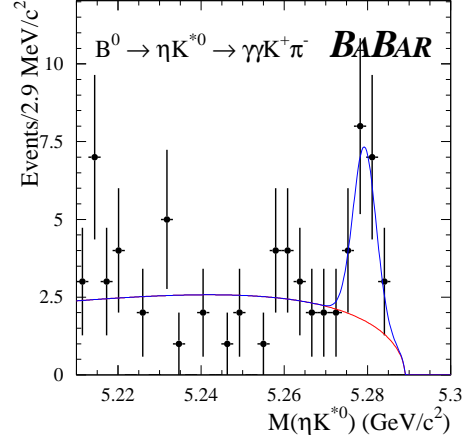


Figure 17. m_{EC} for $B^0 \rightarrow \eta K^{*0}$.

Table 5. Branching fractions for $B^0 \rightarrow \eta K^{*0}$ and $B^+ \rightarrow \eta K^{*+}$. Also shown are the signal yield and significance. An upper limit is also given for $B^+ \rightarrow \eta K^{*+}$.

Mode	Signal yield	S	$\mathcal{B}(\times 10^{-6})$	CL 90 %
ηK^{*0}	21 ± 6	5.4	$19.8^{+6.5}_{-5.6} \pm 1.7$	
ηK^{*+}	14 ± 7	3.2	$22.1^{+11.1}_{-9.2} \pm 3.3$	33.9

are shown in figure 17 and the results for the branching fractions are shown in table 5. For both this analysis and the analysis in the previous section, we confirm the higher than expected branching fractions.

4.4 Evidence for $B^0 \rightarrow a_0^\pm(980)\pi^\mp$

The previously unobserved mode $B^0 \rightarrow a_0^\pm(980)\pi^\mp$ has potential to provide a measurement of $\sin 2\alpha$ in a quasi-two-body analysis. We search for the decay $B^0 \rightarrow a_0^\pm(980)\pi^\mp$ where $a_0 \rightarrow \eta\pi$ and $\eta \rightarrow \gamma\gamma$. A maximum likelihood fit is performed to increase the sensitivity to the signal. The fit includes ΔE , M_η , m_{EC} , as well as Fisher and neural network discriminants based on event shape variables. The dominant background in this channel comes from continuum events. The m_{EC} distribution for this

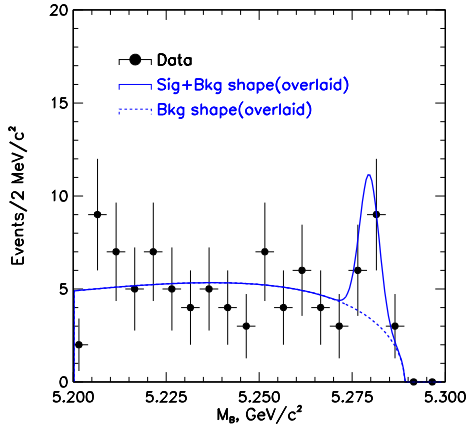


Figure 18. m_{EC} distribution for the decays $B^0 \rightarrow a_0^\pm(980)\pi^\mp$.

mode is shown in figure 18. The fit gives a branching fraction measurement with a 3.7σ significance with a value²² $\mathcal{B}(B^0 \rightarrow a_0^\pm(a_0^\pm \rightarrow \eta\pi^\pm)\pi^\mp) = (6.7_{-2.7}^{+3.2} \pm 1.2) \times 10^{-6}$. This implies an upper limit on the branching fraction of this mode of $\mathcal{B} < 11.2 \times 10^{-6}$ (90% C.L.).

4.5 Measurements of B^0 Decays to $\pi^+\pi^-\pi^0$

The three pion decays of the B^0 offer another method for extracting $\sin 2\alpha$ which exploits the interference between the $B^0 \rightarrow \rho^\mp\pi^\pm$ modes and the colour-suppressed $B^0 \rightarrow \rho^0\pi^0$.²¹ These modes suffer from a large combinatoric background coming from continuum events and small branching fractions. The current analysis²³ uses a Fisher discriminant based on 11 shape variables in order to distinguish between signal and background. Extraction of $\sin 2\alpha$ will require performing an amplitude analysis in the three-pion Dalitz plot. This analysis seeks to measure contributions to the three-pion branching fractions from different regions of the Dalitz plot. The data are sorted into seven samples based on which area of the

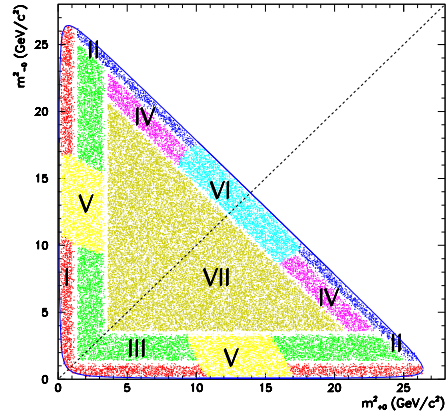


Figure 19. Regions of the three-pion Dalitz plot used for determining branching fractions.

Dalitz plot the three-body decay falls into. Figure 19 shows the regions of the Dalitz plot which are used in the analysis.

A significant signal is seen only in the mode $B^0 \rightarrow \rho^\mp\pi^\pm$ (which corresponds to the regions labelled I in the plot). Upper limits are set for the branching fraction in other regions of the Dalitz plot, and are summarized in table 6.

5 Other Rare B Decays

Rare B decay modes which proceed primarily through penguin or higher-order weak transitions provide an opportunity to search for influences of non-Standard Model processes. These can show up as larger than expected cross sections, or possibly in direct CP-violating effects. With the high luminosity of the B factories it is now possible to begin searching for modes with branching fractions at the 10^{-7} level.

5.1 $B^0 \rightarrow \gamma\gamma$

The decay $B^0 \rightarrow \gamma\gamma$ is expected to occur in the Standard Model at a branching fraction of approximately 10^{-8} , where the con-

Table 6. Results for the three-pion B decay modes in the regions of the Dalitz plot. Shown are the number of signal and background events, the efficiency for the mode, the significance of the result, the branching fraction measurement, and upper limits. A significant result is seen only in the mode $B^0 \rightarrow \rho^+ \pi^-$.

Mode	Signal	Bkgd $q\bar{q} + b\bar{b}$	ϵ	Sig. σ	$\mathcal{B}/10^{-6}$	$\mathcal{B}/10^{-6}$ 90% C.L.
(I) $B^0 \rightarrow \rho^+ \pi^-$	42.8	78.2	0.13	5.0	$28.9 \pm 5.4 \pm 4.3$	
(I) $B^0 \rightarrow \rho^- \pi^+$	46.2	71.8				
(II) $B^0 \rightarrow \rho^0 \pi^0$	6.1	20.9	0.07	1.0	$3.6 \pm 3.5 \pm 1.7$	10.6
(III) $\rho^\pm(1450)$	17.4	57.6	0.15	1.8	$5.1 \pm 2.9 \pm 2.2$	11.3
(IV) $\rho^0(1450)$	-4.7	12.7	0.09			2.7
(V) charged Scalar	8.6	35.4	0.15	0.4	$2.5 \pm 2.1 \pm 0.8$	6.1
(VI) f^0	-0.3	6.3	0.07			5.2
(VII) (NR)	-4.2	45.2	0.07			7.3

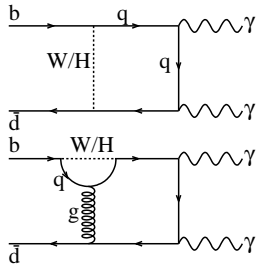


Figure 20. SM Diagrams for $B \rightarrow \gamma\gamma$.

tributing diagrams are shown in figure 20. We look for these events²⁴ by searching for two high energy photons, where at least one photon has $2.3 < E_\gamma < 3.0$ GeV. Photons which can be combined with another photon to create a π^0 candidate are rejected. The m_{ES} versus ΔE plot for events which pass all selections is shown in figure 21. One candidate event lies within the signal box, and we set a branching fraction upper limit $\mathcal{B}(B^0 \rightarrow \gamma\gamma) < 1.7 \times 10^{-6}$, which is more than an order of magnitude improvement on the previous limits.

5.2 $B \rightarrow K\ell^+\ell^-$ and $B \rightarrow K^*(892)\ell^+\ell^-$

The decay $B \rightarrow K\ell^+\ell^-$, which in the Standard Model proceeds via the diagram shown in figure 22, is predicted²⁵ to occur at a branching fraction of order $10^{-7} - 10^{-6}$. These rates are now becoming accessible at

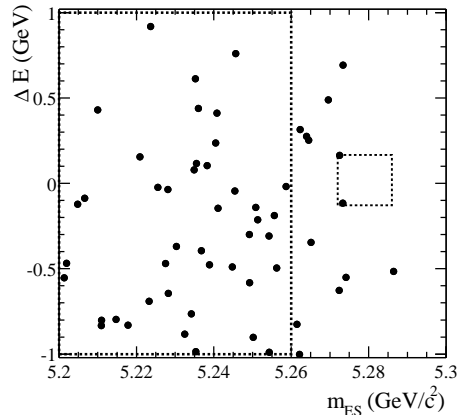
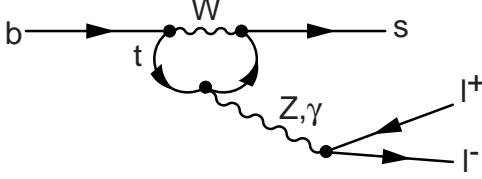
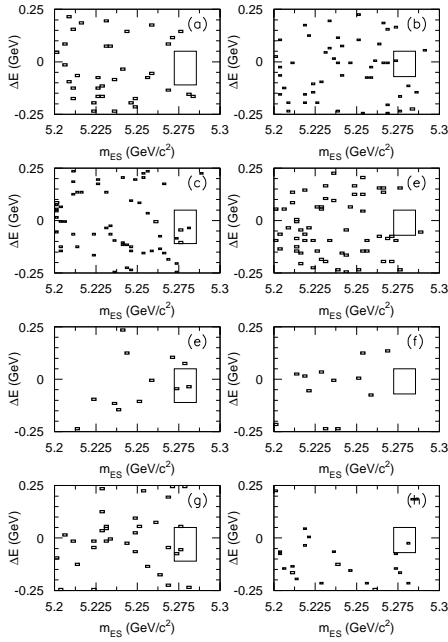


Figure 21. m_{ES} vs ΔE for $B \rightarrow \gamma\gamma$.

the B factories, and we should expect to determine whether the Standard Model predictions are valid.

It is vital to control the backgrounds in this mode as the copious production of $B \rightarrow J/\psi K^{(*)}$ mimics the signal. Events where the invariant mass of the two leptons is consistent with a J/ψ are vetoed. Both the signal and sideband regions for this analysis were kept hidden during the definition of the event selection procedure to avoid bias. The m_{ES} vs ΔE plots for the eight modes studied are shown in figure 23. No evidence for a signal is seen in any of the modes, and we


 Figure 22. Diagram for $B \rightarrow K \ell^+ \ell^-$.

 Figure 23. ΔE vs. m_{ES} for all modes $B \rightarrow K \ell^+ \ell^-$ and $B \rightarrow K^* \ell^+ \ell^-$. The modes are labelled in table 7.

set upper limits of $\mathcal{B}(B \rightarrow K \ell^+ \ell^-) < 0.6 \times 10^{-6}$ at 90% C.L. and $\mathcal{B}(B \rightarrow K^* \ell^+ \ell^-) < 2.5 \times 10^{-6}$ at 90% C.L. which are close to the Standard Model predictions. One could anticipate seeing a signal in this decay mode with the data from the next run of *BABAR* if the Standard Model calculations are correct. A summary of the data is shown in table 7.

5.3 $B \rightarrow K^* \gamma$ Branching Fractions

$B \rightarrow K^* \gamma$ proceeds through a penguin diagram similar to that in figure 22. This mode has the potential to be sensitive to the presence of SUSY or charged Higgs contri-

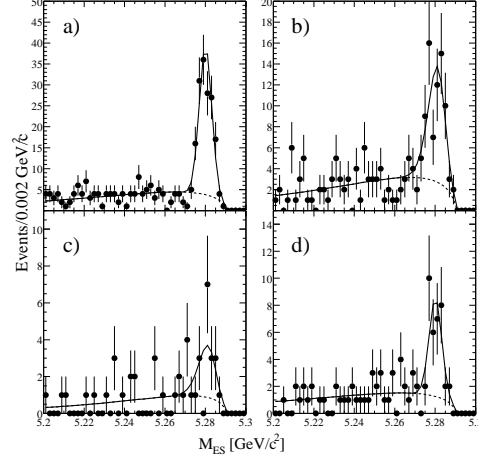

 Figure 24. m_{ES} for each of the $B \rightarrow K^* \gamma$ decay modes. The modes are identified in table 8.

 Table 8. $B \rightarrow K^* \gamma$ branching fractions. Also given are the efficiency and the number of signal events.

Mode	ϵ (%)	Signal	$\mathcal{B}(B \rightarrow K^* \gamma) \times 10^{-5}$
a) $K^+ \pi^-$	14.1	135.7 ± 13.3	$4.39 \pm 0.41 \pm 0.27$
b) $K^+ \pi^0$	5.1	57.6 ± 10.4	$5.52 \pm 1.07 \pm 0.33$
c) $K_S^0 \pi^0$	1.4	14.8 ± 5.6	$4.10 \pm 1.71 \pm 0.42$
d) $K_S^0 \pi^+$	2.9	28.4 ± 6.4	$3.12 \pm 0.76 \pm 0.21$

butions. We have measured the branching fraction into four exclusive modes.²⁷

The main background in this analysis comes from $e^+ e^- \rightarrow q \bar{q} \gamma$ and $e^+ e^- \rightarrow q \bar{q} \rightarrow X \pi^0$, and these events are separated from the signal using the kinematic differences between the signal and background. The m_{ES} measured for the four modes is shown in figure 24, and the branching fractions are summarized in table 8.

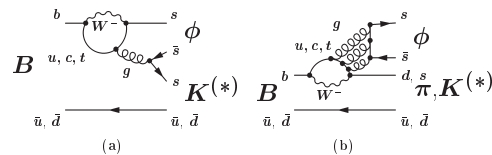

 Figure 25. Penguin diagrams contributing to $B \rightarrow \phi K$ and $B \rightarrow \phi K^*$.

Table 7. Branching fraction upper limits for the modes $B \rightarrow K\ell^+\ell^-$ and $B \rightarrow K^*\ell^+\ell^-$. Also shown are the fitted signal yields, and expected background in each of the modes and the efficiency.

Mode	Signal yield	90% CL yield	Equiv. bkg.	ϵ (%)	$\mathcal{B}/10^{-6}$	$\mathcal{B}/10^{-6}$ 90% CL
(a) $K^+e^+e^-$	-0.2	3.0	0.6	17.5	-0.1	0.9
(b) $K^+\mu^+\mu^-$	-0.2	2.8	0.4	10.5	-0.1	1.3
(c) $K^{*0}e^+e^-$	2.5	6.7	1.8	10.2	1.6	5.0
(d) $K^{*0}\mu^+\mu^-$	-0.3	3.6	1.1	8.0	-0.2	3.6
(e) $K^0e^+e^-$	1.3	5.0	0.3	15.7	1.1	4.7
(f) $K^0\mu^+\mu^-$	0.0	2.9	0.1	9.6	0.0	4.5
(g) $K^{*+}e^+e^-$	0.1	3.8	0.9	8.5	0.1	10.0
(h) $K^{*+}\mu^+\mu^-$	1.0	4.3	0.5	5.8	3.3	17.5

5.4 $B \rightarrow \phi K$ and $B \rightarrow \phi K^*$

The decays $B \rightarrow \phi K$ and $B \rightarrow \phi K^*$ proceed primarily through gluonic penguin diagrams in the Standard Model (figure 25) and so are expected to be sensitive to possible direct CP violating effects. This mode also provides the opportunity for a measurement of $\sin 2\beta$ which is complementary to that from the charmonium modes.

The analysis of this channel²⁸ takes advantage of the excellent kaon ID in *BABAR* for high momentum kaons in order to reduce backgrounds. A maximum likelihood fit is performed using m_{ES} , ΔE , and M_{KK} as well as measurements of the particle ID in the DIRC, and kinematic discriminants. Results of the fits are given in table 9. Signals have been seen in four modes, including the first observations of ϕK^{*+} and ϕK^0 . The projection of m_{ES} is shown in figure 26 for these modes.

6 Semileptonic B Decays

The large samples of fully reconstructed B decays at the B factories allow us to explore new methods of reducing systematic uncertainties in measuring semileptonic decay rates. In the *BABAR* Run 1 data sample there are approximately 14,000 fully reconstructed B decays in about equal amounts of charged

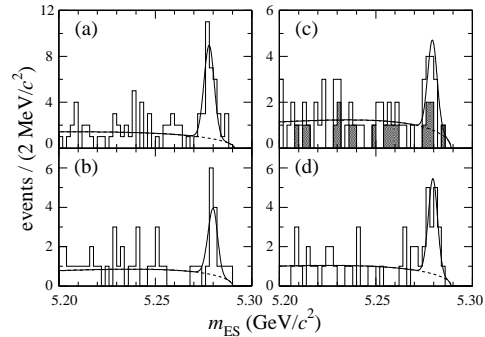


Figure 26. m_{ES} projections for $B \rightarrow \phi K$ and $B \rightarrow \phi K^*$ decay modes.

Table 9. Measured branching fractions for $B \rightarrow \phi K$ and $B \rightarrow \phi K^*$ decay modes. Also shown are the efficiency, the number of signal events, and the significance of the result.

Mode	ϵ	n_{sig}	S	$\mathcal{B}(10^{-6})$
(a) ϕK^+	17.9	$31.4^{+6.7}_{-5.9}$	10.5	$7.7^{+1.6}_{-1.4} \pm 0.8$
(b) ϕK^0	6.1	$10.8^{+4.1}_{-3.3}$	6.4	$8.1^{+3.1}_{-2.5} \pm 0.8$
(c) ϕK^{*+}	4.9	—	4.5	$9.7^{+4.2}_{-3.4} \pm 1.7$
(d) ϕK^{*0}	8.6	$16.9^{+5.5}_{-4.7}$	6.6	$8.6^{+2.8}_{-2.4} \pm 1.1$
$\phi\pi^+$	19.1	$0.9^{+2.1}_{-0.9}$	0.6	< 1.4 (90% CL)

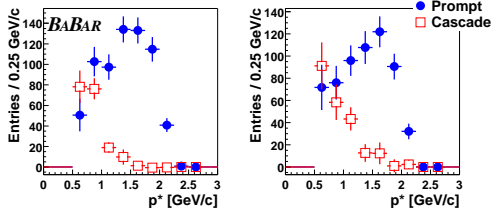


Figure 27. Momentum spectra for prompt and cascade leptons for B^0 (left) and B^+ (right) decays.

and neutral B states. For the charged B the largest branching fraction modes are $B^0 \rightarrow D^{(*)-}\pi^+$, $D^{(*)-}\rho^+$, $D^{(*)-}a_1^+$, $J/\psi K^{*0}$ while for the neutral B $B^+ \rightarrow \bar{D}^{(*)0}\pi^+$, $J/\psi K^+$, $\psi(2S)K^+$ provide the largest number of events. Once a B is fully reconstructed, it is possible to determine whether the lepton found in the other B in the event was a prompt lepton or a cascade lepton. This gives an independent measure of the prompt and cascade momentum spectra. The overall number of prompt and cascade events for charged B decays is given by $N_{right-sign}^+ = N_p^+$, $N_{wrong-sign}^+ = N_c^+$. For neutral B decays, there is a dilution due to the mixing, χ_d , which is accommodated as $N_{right-sign}^0 = N_p^0(1 - \chi_d) + N_c^0\chi_d$, $N_{wrong-sign}^0 = N_p^0\chi_d + N_c^0(1 - \chi_d)$.

Figure 27 shows the momentum spectra extracted from the Run 1 data. The measured branching fractions are $\mathcal{B}(B^+ \rightarrow e^- X) = (10.3 \pm 0.6 \pm 0.5)\%$ and $\mathcal{B}(B^0 \rightarrow e^- X) = (10.4 \pm 0.8 \pm 0.5)\%$ which give

$$\mathcal{B}(B \rightarrow e^- X) = (10.4 \pm 0.5 \pm 0.4)\%$$

$$\frac{\mathcal{B}(B^+ \rightarrow e^- X)}{\mathcal{B}(B^0 \rightarrow e^- X)} = (0.99 \pm 0.10 \pm 0.03)\%$$

7 B Lifetimes, Mixing, and Searches for Direct CP Violation

7.1 B Lifetimes

Using fully reconstructed B decays also gives a substantial reduction on the error in de-

termining the B^0 and B^+ lifetimes. The B factories require new techniques in order to extract the B lifetimes as the centre-of-mass is boosted in the lab frame and there is no knowledge of the production point of the Bs. Instead one needs to measure the difference in flight length which is directly sensitive to the lifetime. *BABAR* uses the sample of fully reconstructed B decays with which one can vertex and tag one B as either B^0 or B^+ . The tracks in the event not associated with the fully reconstructed B are inclusively vertexed to form the estimated decay point of the other B. The knowledge of the beamspot position is used to improve this vertex. The width of the distribution of the decay times differences is a combination of the detector resolution and the B lifetimes. These distributions are shown in figure 28, and are fit simultaneously in order to extract the B^0 and B^+ lifetimes.²⁹ The results of the fit are

$$\tau_{B^0} = 1.546 \pm 0.032 \pm 0.022 \text{ ps,}$$

$$\tau_{B^+} = 1.673 \pm 0.032 \pm 0.023 \text{ ps,}$$

$$\tau_{B^+}/\tau_{B^0} = 1.082 \pm 0.026 \pm 0.012$$

which are the best single measurements of these lifetimes.

7.2 B Mixing with Leptons

Events in which both Bs decay semileptonically allow one to measure the B mixing parameter Δm_d by measuring the time dependent difference in the like sign vs unlike sign lepton events. Measuring this asymmetry

$$A(\Delta t) = \frac{N(\ell^+\ell^-)(\Delta t) - N(\ell^\pm\ell^\pm)(\Delta t)}{N(\ell^+\ell^-)(\Delta t) + N(\ell^\pm\ell^\pm)(\Delta t)}$$

we extract³⁰ $\Delta m_d = 0.499 \pm 0.010 \pm 0.012 \text{ } \hbar \text{ ps}^{-1}$ from the data shown in figure 29.

It is also possible to search for CP/T violation in mixing, measuring ϵ_B from the

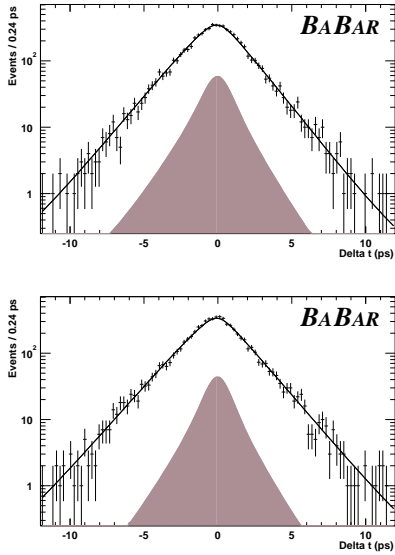


Figure 28. Δt for B^0 (top) and B^+ (bottom). The shaded area indicates the background.

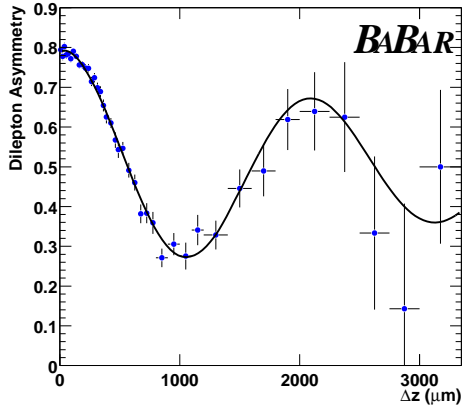


Figure 29. Time-dependent asymmetry for dilepton events $A(\Delta t)$.

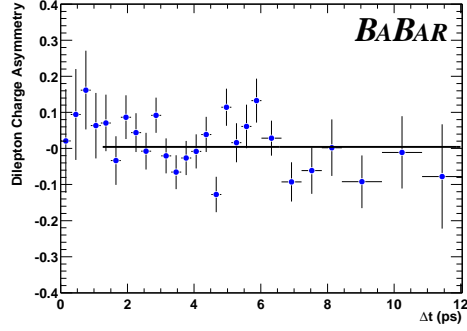


Figure 30. Time-dependent dilepton charge asymmetry $A_t(\Delta t)$.

dilepton charge asymmetry

$$A_t(\Delta t) = \frac{N(\ell^+\ell^+)(\Delta t) - N(\ell^-\ell^-)(\Delta t)}{N(\ell^+\ell^+)(\Delta t) + N(\ell^-\ell^-)(\Delta t)}$$

$$\approx \frac{4\text{Re}(\epsilon_B)}{1 + |\epsilon_B|^2}$$

ϵ_B is the equivalent in the B system to the parameter ϵ in the K system. The data for $A_t(\Delta t)$ are shown in figure 30. Measuring $A_t(\Delta t)$ we find ³²

$$\frac{\text{Re}(\epsilon_B)}{1 + |\epsilon_B|^2} = (0.12 \pm 0.29 \pm 0.36)\%$$

which is the most stringent test of CP violation in B mixing.

7.3 Searches for Direct CP Violation

Direct CP violation can be observed if there is a difference in both the weak and strong phases between two different diagrams to the same final state. This effect can be searched for by looking for a charge asymmetry in the observed final states. One forms the asymmetry

$$\mathcal{A}_{CP} = \frac{\mathcal{B}(\overline{B} \rightarrow \overline{f}) - \mathcal{B}(B \rightarrow f)}{\mathcal{B}(\overline{B} \rightarrow \overline{f}) + \mathcal{B}(B \rightarrow f)}$$

$\approx |A_1||A_2| \sin \Delta\phi_W \sin \Delta\phi_S$ which is sensitive to any direct CP violating effects. Currently we see no evidence for direct CP violation³¹, and a summary of the limits we set are shown in table 10.

Table 10. summary of limits on direct CP violation in modes studied by *BABAR*.

$$\begin{aligned}
\mathcal{A}_{\mathcal{CP}}(\eta' K^\pm) &= -0.11 \pm 0.11 \pm 0.02 \\
\mathcal{A}_{\mathcal{CP}}(\omega \pi^\pm) &= -0.01_{-0.31}^{+0.29} \pm 0.03 \\
\mathcal{A}_{\mathcal{CP}}(\phi K^\pm) &= -0.05 \pm 0.20 \pm 0.03 \\
\mathcal{A}_{\mathcal{CP}}(\phi K^{*\pm}) &= -0.43_{-0.30}^{+0.36} \pm 0.06 \\
\mathcal{A}_{\mathcal{CP}}(\phi K^{*0}) &= 0.00 \pm 0.27 \pm 0.03 \\
&K^* \gamma \\
\mathcal{A}_{\mathcal{CP}}(K^\pm \pi^\mp \gamma) &= -0.035 \pm 0.094 \pm 0.022 \\
\mathcal{A}_{\mathcal{CP}}(K_s^0 \pi^\pm \gamma) &= -0.19 \pm 0.21 \pm 0.012 \\
\mathcal{A}_{\mathcal{CP}}(K^\pm \pi^0 \gamma) &= 0.044 \pm 0.155 \pm 0.021 \\
\mathcal{A}_{\mathcal{CP}}(K^* \gamma) &= -0.035 \pm 0.076 \pm 0.012 \\
&J/\psi K^\pm \\
\mathcal{A}_{\mathcal{CP}}(J/\psi K^\pm) &= 0.004 \pm 0.029 \pm 0.004
\end{aligned}$$

8 Conclusions

The first Run of *BABAR* has provided a glimpse at the potential of the B factories for providing detailed tests of the CKM sector of the Standard Model as well as probing for possible effects beyond those predicted by the Standard Model. The second Run of *BaBar* is now underway and will continue until July 2002. By the end of this Run it is anticipated that *BABAR* will have recorded 100/fb of data providing a rich sample to continue the search for rare B decays, and measure CP violating effects in a variety of B decay modes. As can be seen by the impressive results shown by our colleagues at KEK today¹⁴, we expect a healthy competition in compiling these results.

Acknowledgments

It is a pleasure to acknowledge the conference organizers for the delightful meeting in Rome. I would also like to acknowledge our colleagues at PEP II for providing the out-

standing machine performance which enabled us to produce these results.

References

1. B. Aubert *et al.* [BABAR Collaboration], arXiv:hep-ex/0105044. To be published in NIM.
2. J. Dorfan, these proceedings.
3. B. Aubert *et al.* [BABAR Collaboration], Phys. Rev. Lett. **87** (2001) 091801 [arXiv:hep-ex/0107013].
4. S. Olsen, these proceedings.
5. B. Aubert *et al.* [BABAR Collaboration], Phys. Rev. Lett. **87** (2001) 162002 [arXiv:hep-ex/0106044].
6. B. Aubert *et al.* [BABAR Collaboration], arXiv:hep-ex/0107025.
7. B. Aubert *et al.* [BABAR Collaboration], arXiv:hep-ex/0108009.
8. B. Aubert *et al.* [BABAR Collaboration], Phys. Rev. Lett. **87** (2001) 241801 [arXiv:hep-ex/0107049].
9. CLEO Collaboration, CLEO CONF 97-26, EPS97 337.
10. ALEPH Collaboration, R. Barate *et al.*, Eur. Phys. J. **C4**, 387-407 (1998).
11. G. Buchalla, I. Dunietz and H. Yamamoto, Phys. Lett. **B364**, 188 (1995).
12. B. Aubert *et al.* [BABAR Collaboration], arXiv:hep-ex/0107056.
13. B. Aubert *et al.* [BABAR Collaboration], arXiv:hep-ex/0107057.
14. H. Tajima, these proceedings.
15. B. Aubert *et al.* [BABAR Collaboration], Phys. Rev. Lett. **87** (2001) 151802 [arXiv:hep-ex/0105061], B. Aubert *et al.* [BABAR Collaboration], arXiv:hep-ex/0109005.
16. CLEO Collaboration, S. J. Richichi *et al.* Phys. Rev. Lett. **85**, 520 (2000); CLEO CONF 99-12 (1999).
17. B. Aubert *et al.* [BABAR Collaboration], Phys. Rev. Lett. **87** (2001) 221802 [arXiv:hep-ex/0108017].
18. CLEO Collaboration S.J. Richichi *et al.*,

- Phys. Rev. Lett. **85**, 520 (2000);
CLEO CONF 99-12 (1999).
19. A. Ali, G. Kramer, and C.D. Lü, Phys. Rev. D **58**, 094009 (1998);
Y. H. Chen *et al.*, Phys. Rev. D **60**, 094014 (1999).
20. B. Aubert *et al.* [BABAR Collaboration], arXiv:hep-ex/0107037.
21. P. F. Harrison and H. R. Quinn [BABAR Collaboration], SLAC-R-0504.
22. B. Aubert *et al.* [BABAR Collaboration], arXiv:hep-ex/0107075.
23. B. Aubert *et al.* [BABAR Collaboration], arXiv:hep-ex/0107058.
24. B. Aubert *et al.* [BABAR Collaboration], Phys. Rev. Lett. **87** (2001) 241803 [arXiv:hep-ex/0107068].
25. A. Ali, P. Ball, L.T. Handoko, and G. Hiller, Phys. Rev. D **61**, 074024 (2000); hep-ph/9910221.
T.M. Aliev, A. Ozpineci and M. Savci, Phys. Rev. D **56**, 4260 (1997); hep-ph/9612480.
T.M. Aliev, C.S. Kim, and Y.G. Kim, Phys. Rev. D **62**, 014026 (2000); hep-ph/9910501.
D. Melikhov, N. Nikitin, and S. Simula, Phys. Lett. B **410**, 290 (1997); hep-ph/9704628.
D. Melikhov and B. Stech, Phys. Rev. D **62**, 014006 (2000); hep-ph/0001113.
P. Colangelo, F. De Fazio, P. Santorelli, and E. Scrimieri, Phys. Rev. D **53**, 3672 (1996); Erratum-*ibid.* D**57**, 3186 (1998); hep-ph/951043.
P. Colangelo *et al.*, Eur. Phys. J. C **8**, 81 (1999); hep-ph/9809372.
26. B. Aubert *et al.* [BABAR Collaboration], arXiv:hep-ex/0107026.
27. B. Aubert *et al.* [BABAR Collaboration], arXiv:hep-ex/0110065.
28. B. Aubert *et al.* [BABAR Collaboration], Phys. Rev. Lett. **87** (2001) 151801 [arXiv:hep-ex/0105001].
29. B. Aubert *et al.* [BABAR Collaboration], Phys. Rev. Lett. **87** (2001) 201803 [arXiv:hep-ex/0107019].
30. B. Aubert *et al.* [BABAR Collaboration], arXiv:hep-ex/0008054.
31. B. Aubert *et al.* [BABAR Collaboration], arXiv:hep-ex/0109006.
32. B. Aubert *et al.* [BABAR Collaboration], arXiv:hep-ex/0107059.